Hindawi Publishing Corporation
ISRN Geophysics
Volume 2013, Article ID 496352, 8 pages
http://dx.doi.org/10.1155/2013/496352

Research Article

Streaming Potential and Electroosmosis Measurements to Characterize Porous Materials

D. T. Luong and R. Sprik

Van der Waals-Zeeman Institute, University of Amsterdam, 1098 XH Amsterdam, The Netherlands

Correspondence should be addressed to R. Sprik; r.sprik@uva.nl

Received 22 April 2013; Accepted 24 May 2013

Academic Editors: E. Liu, A. Streltsov, and A. Tzanis

Characterizing the streaming potential and electroosmosis properties of porous media is essential in applying seismoelectric and electroseismic phenomena for oil exploration. Some parameters such as porosity, permeability, formation factor, pore size, the number of pores, and the zeta potential of the samples can be obtained from elementary measurements. We performed streaming potential and electro-osmosis measurements for 6 unconsolidated samples made of spherical polymer particles. To check the validity of the measurements, we also used alternative analysis to determine the average pore size of the samples and, moreover, used a sample made of sand particles to determine the zeta potential.

1. Introduction

Recently, seismoelectric and electroseismic conversions which arise due to the coupling of seismic waves and electromagnetic waves have been studied in order to investigate oil and gas reservoirs [1] or hydraulic reservoirs [2–4]. These phenomena have been used to deduce the depth and the geometry of the reservoir [5]. The coupling coefficients of conversion between electric wave and flow depend strongly on the fluid conductivity, porosity, permeability, formation factor, pore size, zeta potential of porous media, and other properties of the rock formation [6]. Therefore, determining these parameters is very important in studying electrokinetics in general and to model seismoelectric and electroseismic conversions. Li et al. [7] used two reciprocal electrokinetic phenomena known as streaming potential and electro-osmosis by Ac measurement to determine the effective pore size and permeability of porous media. In [8], the authors used image analysis to determine the number of pores per cross-sectional area of porous samples (see Figure 1 for the schematic of the porous medium with different length scales). This parameter is especially important in processes of contaminant removal from low-permeability porous media under a Dc electric field [8], and in building electro-osmosis micropumps [9].

However, the method used in [8] did not work for porous media with very small pores such as Bentonite clay soils or tight-gas sandstones (the pore radius is smaller than 1 μm) that are relevant for application in the oil and gas industry. In oil exploration and production, the typical pore sizes in rocks are necessary information for considering the location of oil and fluid flow through the rocks. The characteristics of porous media also determine differential gas pressures needed to overcome capillary resistance of tight-gas sandstones in gas production

Alternative methods such as nuclear magnetic resonance (NMR) or magnetic resonance imaging (MRI) [10] can also be used to determine characteristics of porous media such as the porosity and pore size distribution, the permeability, and the water saturation. But this technique is quite expensive and is not able to determine the zeta potential—one of the most important parameters in electrokinetic phenomena.

Here we used Dc measurements of streaming potential and electro-osmosis in porous samples and other simple measurements to fully characterize porous media and determine parameters needed for the experimental study of seismoelectric and electroseismic conversions. Our approach works well for very small pores in particular.

This work includes five sections. Section 2 describes the theoretical background of electrokinetics. Section 3 presents

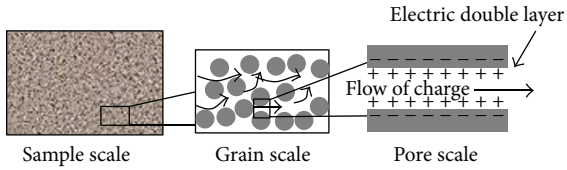

Figure 1: Schematic of the porous medium with different length scales: sample scale, grain scale, and pore scale.

the investigated samples and the experimental methods. Section 4 contains the experimental results and their interpretation using the model proposed by [11]. Conclusions are provided in Section 5.

2. Theoretical Background of Electrokinetics

2.1. Electric Double Layer. Electrokinetic phenomena are induced by the relative motion between the fluid and a wall, and they are directly related to the existence of an electric double layer (EDL) between the fluid and the solid surface. When a solid surface is in contact with a liquid, an electric field is generated perpendicular to the surface which attracts counterions (usually cations) and repulses anions in the vicinity of the liquid-solid interface. This leads to the charge distribution known as the EDL. The EDL is made up of the Stern layer, where cations are adsorbed on the surface and are immobile due to the strong electrostatic attraction, and the Gouy diffuse layer, where the ions are mobile. In the bulk liquid, the number of cations and anions is equal so that it is electrically neutral. The closest plane to the solid surface in the diffuse layer at which flow occurs is termed the shear plane or the slipping plane, and the electrical potential at this plane is called the zeta potential. The characteristic length over which the EDL strongly exponentially decays is known as the Debye length, and it is on the order of a few nanometers for typical grain electrolyte combinations [6] (for more detail, see [12–14]).

2.2. Streaming Potential. The streaming current is created by the motion of the diffuse layer with respect to the solid surface induced by a fluid pressure drop over the channel. This streaming current is then balanced by a conduction current, leading to the streaming potential. In a porous medium (see Figure 1), the electric current density and the fluid flux are coupled, so fluids moving through porous media generate a streaming potential [15]. The streaming potential increases linearly with the fluid pressure difference that drives the fluid flow, provided that the flow remains laminar [16]. The steady-state streaming potential coupling coefficient, C_S, is defined when the total current density is zero as follows:

$$C_S = \frac{\Delta V}{\Delta P} = \frac{\epsilon\zeta}{\eta\sigma_{\text{eff}}}, \tag{1}$$

where ΔV is the streaming potential, ΔP is the fluid pressure difference, ϵ is the dielectric permittivity of the fluid, η is the dynamic viscosity of the fluid, ζ is the zeta potential, and σ_{eff} is the effective conductivity which includes the intrinsic fluid conductivity and the surface conductivity (that is due to the electric double layer and the surface itself). The streaming potential is independent of the sample geometry.

According to [15], C_S can be written as

$$C_S = \frac{\epsilon\zeta}{\eta\sigma_{\text{eff}}} = \frac{\epsilon\zeta}{\eta F\sigma_S}, \tag{2}$$

where σ_S is the electrical conductivity of the sample saturated with a fluid with a conductivity σ_f and F is the formation factor. If surface conductivity is negligible, then $\sigma_{\text{eff}} = \sigma_f$ and the coupling coefficient becomes the equation

$$C_S = \frac{\epsilon\zeta}{\eta\sigma_f}. \tag{3}$$

2.3. Electroosmosis. Electroosmosis was first observed by Reuss in 1809 in an experiment where a direct current was applied to a clay-sand-water mixture in a U-tube [17]. When an electric field is applied parallel to the wall of a capillary, ions in the diffuse layers experience a Coulomb force and move toward the electrode of opposite polarity, which creates a motion of the fluid near the wall and transfers momentum via viscous forces into the bulk liquid. So a net motion of bulk liquid along the wall is created and is called electroosmosis flow.

A complex porous medium (see Figure 1) with the physical length L and cross-sectional area A can be approximated as an array of N parallel capillaries with inner radius equal to the average pore radius a of the medium and an equal value of zeta potential ζ. For each of these idealized capillaries, the solution for electro-osmosis flow in a single tube can be analyzed to estimate the behavior of the total flow in a porous medium by integrating over all pores [18].

In a U-tube experiment, when potential difference is applied across the fluid-saturated porous medium, the liquid rises on one side (the cathode compartment for our experiment) and lowers on the other side (the anode compartment). This height difference increases with the time, and this process stops when the hydraulic pressure caused by the height difference equals the electro-osmosis pressure (see Figure 2). At that time, the height difference is maximum.

The expression for the height difference as function of time is given by [8]

$$\begin{aligned}\Delta h &= \frac{\Delta P_{\text{eq}}}{\rho_f g}\left[1 - \exp\left(-\frac{N\rho_f g a^4}{4\mu R^2 L}t\right)\right] \\ &= \frac{\Delta P_{\text{eq}}}{\rho_f g}\left[1 - \exp\left(-\frac{t}{\tau}\right)\right],\end{aligned} \tag{4}$$

with

$$\Delta P_{\text{eq}} = \frac{8\epsilon\,|\zeta|\,V}{a^2}\left[1 - \frac{2\lambda I_1(a/\lambda)}{aI_0(a/\lambda)}\right], \tag{5}$$

$$\tau = \frac{4\mu R^2 L}{N\rho_f g a^4}, \tag{6}$$

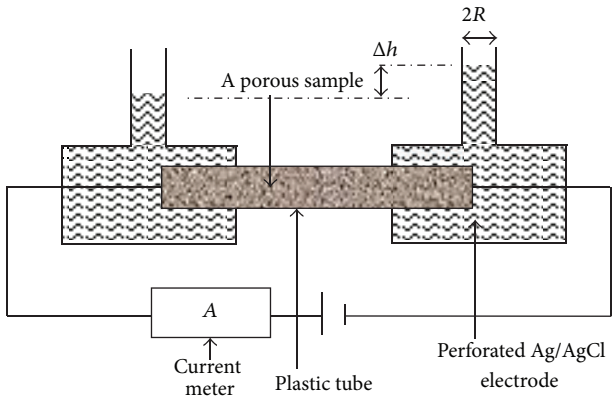

Figure 2: Experimental setup for electro-osmosis measurements in which Δh and R are height difference of liquid and the radius of the tubes in both sides, respectively.

where τ is response time, ΔP_{eq} is the pressure difference caused by the electro-osmosis flow at equilibrium which corresponds to maximum height difference, V is the applied voltage across the porous medium, ρ_f is the fluid density, g is the acceleration due to gravity, λ is the Debye length, R is the radius of the tubes in both sides, and I_0 and I_1 are the zero-order and the first-order modified Bessel functions of the first kind, respectively.

For a conductive liquid such as distilled water, the Debye length λ is about 2 nm [8], and a typical pore radius of our samples a (see below) is around 3 μm in this case; the ratio $I_1(a/\lambda)/I_0(a/\lambda)$ can be neglected [19]. Under these conditions, (5) may be simplified as

$$\Delta P_{\text{eq}} = \frac{8\epsilon\,|\zeta|\,V}{a^2}, \tag{7}$$

and (4) can be rewritten as follows:

$$\Delta h = \frac{8\epsilon\,|\zeta|\,V}{\rho_f g a^2}\left[1 - \exp\left(-\frac{t}{\tau}\right)\right] = \Delta h_{\max}\left[1 - \exp\left(-\frac{t}{\tau}\right)\right], \tag{8}$$

with

$$\Delta h_{\max} = \frac{8\epsilon\,|\zeta|\,V}{\rho_f g a^2}. \tag{9}$$

3. Experiment

To demonstrate that one can characterize porous media by obtaining parameters such as porosity, permeability, formation factor, pore size, the number of pores, and zeta potential of the liquid fully saturated porous media through electrokinetics, streaming potential and electro-osmosis measurements have been performed on 7 unconsolidated samples. Six of them are spherical monodisperse particle packs with different diameters (10 μm, 20 μm, 40 μm, 140 μm, 250 μm, and 500 μm) of the particles. These are obtained from Microbeads AS Company, and they are composed of polystyrene polymers. Those samples are designated as TS10, TS20, TS40, TS140, TS250, and TS500, respectively. We also used an unconsolidated sample made up of blasting sand particles obtained from Unicorn ICS BV Company with diameter in the range of 200–300 μm, and this is designated as S_{sand}.

When using low electrical conductivity solutions such as deionized water, the magnitude of the coupling coefficient is large. The electrical conductivity of the saturated samples slowly stabilizes in about 24 h for our samples. Perhaps due to CO_2 uptake from the air, that changes the conductivity. We, therefore, use a 10^{-3} M NaCl solution of low enough conductivity of 10×10^{-3} S/m measured by the conductivity meter (Consort C861) for the measurements. All measurements were carried out at room temperature (20°C).

3.1. Sample Assembly. Samples were constructed by filling polycarbonate plastic tubes (1 cm in inner diameter and 7.5 cm in length) successively with 2 cm thick layers of particles that were gently tamped down, and they were then shaken by a shaker (TIRA-model TV52110). Filter paper was used in both ends of the tube to retain the particles and is permeable enough to let the fluid pass through. The samples were flushed with deionized water to remove any powder or dust.

3.2. Porosity, Permeability, and Formation Factor Measurements. The porosity was measured by a simple method [9]. The sample was first dried in oven for 24 hours, then cooled to room temperature, and finally fully saturated with deionized water under vacuum. The sample was weighed before (m_{dry}) and after saturation (m_{wet}), and the porosity was determined as

$$\phi = \frac{\left(m_{\text{wet}} - m_{\text{dry}}\right)/\rho}{AL}, \tag{10}$$

where ρ is density of the deionized water and A and L are the inner cross-sectional area and the physical length of the tubing, respectively.

The permeability k was measured by constant flow-rate method. A high-pressure pump (LabHut, Series III-Pump) ensures a constant flow through the sample, and a high-precision differential pressure transducer (Endress and Hauser Deltabar S PMD75) is used to measure the pressure drop. At different flow rates the pressure drop was measured to determine the permeability of the sample.

Method of determining the tortuosity was proposed in [20]. They defined the formation factor F as

$$F = \frac{\alpha_\infty}{\phi} = \frac{\sigma_f}{\sigma_S}, \tag{11}$$

where α_∞ is the tortuosity, σ_S is the electrical conductivity of the saturated sample, σ_f is the intrinsic fluid conductivity, and ϕ is the porosity of the sample.

Our experimental setup is similar to the one used in [21] and is shown in Figure 3. The electrodes, Ag/AgCl mesh discs,

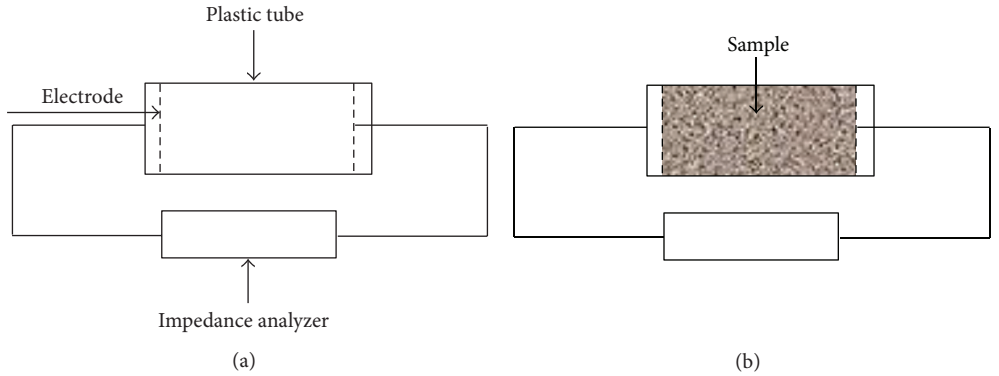

Figure 3: Setup for measuring the electrical conductivity of a porous medium saturated with an electrolyte on the right. On the left-hand side is the identical setup without the porous medium for measuring the fluid conductivity.

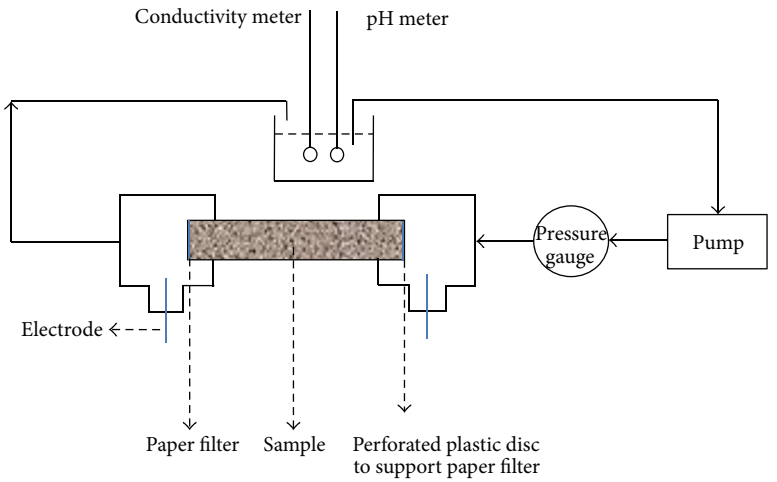

Figure 4: Experimental setup for streaming potential measurements.

were placed on both sides against the porous sample that was saturated successively with the following set of aqueous NaCl solutions with different conductivities (0.13, 0.47, 0.81, 1.23, 1.51, and 1.98 S/m). For consolidated sandstone cores, when the electrical conductivity of solution is higher than 0.60 S/m, the surface conductivity is negligible [22]. According to [16], the surface conductivity is around 0.43 mS/m for a 50–60 μm sand pack and is inversely proportional to the grain diameter. For the materials we used, it is likely that the surface conductivity is smaller than that of traditional materials such as sand or sandstone, so that the surface conductivity can also be neglected for our experiments. The electrical conductivity was measured using a Hioki IM3570 impedance analyzer at different frequencies (varying from 100 Hz to 100 kHz).

3.3. Streaming Potential Measurement. The experimental setup for the measurement of the streaming potential is shown in Figure 4. The pressure differences across the sample were created by the high-pressure pump and were measured by the pressure transducer. The electrical potential was measured by two Ag/AgCl wire electrodes (A-M systems). The electrodes were put in the vicinity of the end faces of the sample but not within the liquid circulation to avoid the electrical noise from liquid movement around the electrodes [15].

The tubing circuit is shown in Figure 4; the electrolyte from the outlet tube is not in contact with the electrolyte used to pump liquid through the samples, preventing an electric current leakage through the liquid in the tube. The solution was circulated through the samples until the electrical conductivity and pH of the solution reached a stable value. Electrical potentials across the samples were then measured by a high-input impedance multimeter (Agilent 34401A) connected to a computer and controlled by a Labview program (National Instruments). The electrical potentials at a given pressure difference fluctuate around a specific value (see Figure 7); the Labview program averages the value of electrical potentials. The pH values of equilibrium solutions, measured with the pH meter (Consort C861), are in the range 7.1 to 7.6, and the solutions were also used for electro-osmosis measurements.

3.4. Electroosmosis Measurement. The experimental setup for the electro-osmosis measurement is shown in Figure 2. The

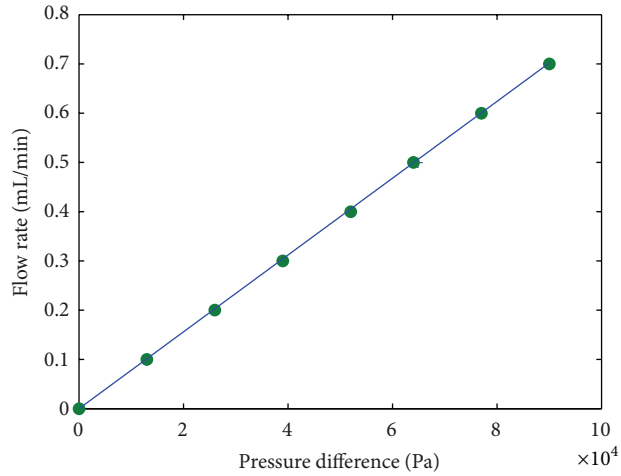

Figure 5: The flow rate against pressure difference. Two runs are shown for sample TS10.

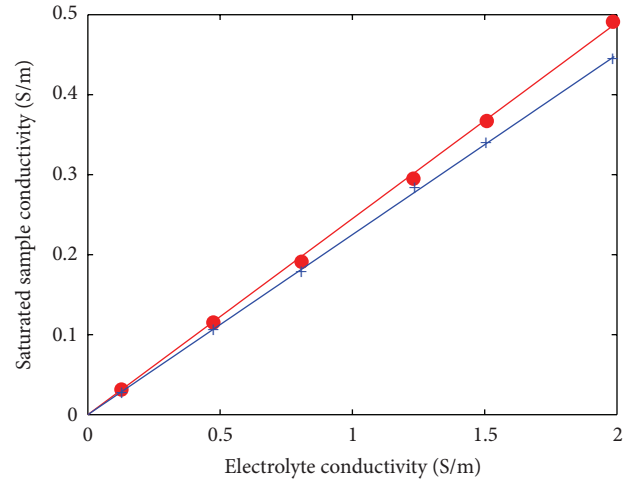

Figure 6: Saturated sample conductivity versus electrolyte conductivity for 2 samples (red dots for TS10 and blue cross symbols for TS500). The slopes of the straight lines yield the formation factors.

same solution used in the streaming potential measurement was also used for this measurement. The zeta potential is consequently the same for both kinds of measurements. The electrodes used to apply a Dc voltage across the samples are perforated Ag/AgCl electrodes (MedCaT). To measure the maximum height difference, $\Delta h_{\max}$, and the height difference as a function of time at a given voltage, cameras (Philips SPC 900NC PC) with the assistance of HandiAVI software were used to take pictures of the heights of the liquid columns in time. For each new measurement (new applied voltage, new sample), the samples were dried, mounted in the setup, evacuated by a vacuum pump, and fully saturated by the same solutions.

It should be noted that, when an applied voltage exceeds a critical value (1.48 V for water [23]), there will be electrolysis at the anode and the cathode. These electrode reactions produce ions and gas in both electrodes. If these ions are not removed, then these reactions induce a low pH at the anode, a high pH at the cathode, and a change in electrical conductivity. The rate of electrolysis reaction is largely determined by the current. If the current density is smaller than $<35\,\mu$A per cm^2 cross-sectional area, then the effects due to the electrolysis can be ignored [24]. The resistances of the fully saturated samples that we used in this paper are about 400 kΩ, so applied voltages were limited below 10 V to avoid unwanted electrolysis effects.

4. Results and Discussion

4.1. Porosity, Permeability, and Formation Factor. The measured porosity of the packs as mentioned in Section 3.2 is 0.39 independently of the size of the particles with an error of 5%. Figure 5 shows the typical graph of flow rate as a function of applied pressure difference for sample TS10.

The graph shows that there is a linear relationship between flow rate and pressure difference, and Darcy's law is obeyed. So the flow is laminar, and (1) and (2) are valid. This behavior is identical for all samples. Two measurements were performed for all samples to find the graphs of flow rate versus pressure difference. From the slope of the graph and Darcy's law (the viscosity of the fluid was taken as 10^{-3} Pa.s), the permeability of the sample was calculated. We obtained permeabilities of all samples (see Table 1) with an uncertainty of 15% in the reported values.

Table 1: Measured properties of the samples in which d, k_o, F, and σ_S are diameter, permeability, formation factor, and electrical conductivity of the fully saturated sample at equilibrium for all samples, respectively.

Sample	d (in μm)	k_o (in m^2)	F	σ_S (in S/m)
TS10	10	0.15×10^{-12}	4.0	4.1×10^{-3}
TS20	20	0.30×10^{-12}	4.2	3.6×10^{-3}
TS40	40	0.85×10^{-12}	4.2	3.0×10^{-3}
TS140	140	1.36×10^{-12}	4.3	3.1×10^{-3}
TS250	250	1.71×10^{-12}	4.0	3.5×10^{-3}
TS500	500	2.36×10^{-12}	4.3	2.9×10^{-3}
S_{sand}	200–300	1.22×10^{-12}	4.0	3.0×10^{-3}

An example of the electrical conductivity of the samples versus the electrical conductivity of the electrolyte is shown in Figure 6 for the 2 samples with the largest differences in the formation factors. We calculated the formation factor F as the reciprocal of the slope of a linear regression through the data points. Values of the formation factors for all samples are also reported in Table 1 with the 5% error.

The measured formation factor of the samples is the range from 4.0 to 4.3 (see Table 1). According to Archie's law, $F = \phi^{-m}$ (F is the formation factor, ϕ is the porosity of the sample, and m is the socalled cementation exponent), m was found to be in the range 1.47–1.55. For unconsolidated samples made of perfect spheres, the exponent m should be 1.5 [25]. So the measured formation factors of the samples are in good agreement with Archie's law. The electrical conductivities of the samples fully saturated by the solutions are also shown in Table 1.

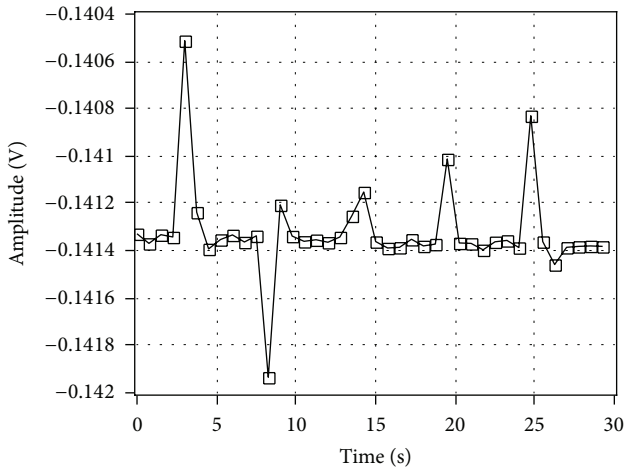

Figure 7: The electrical potential (V) fluctuating with time (s) at a given pressure drop for sample TS10 was taken by Labview.

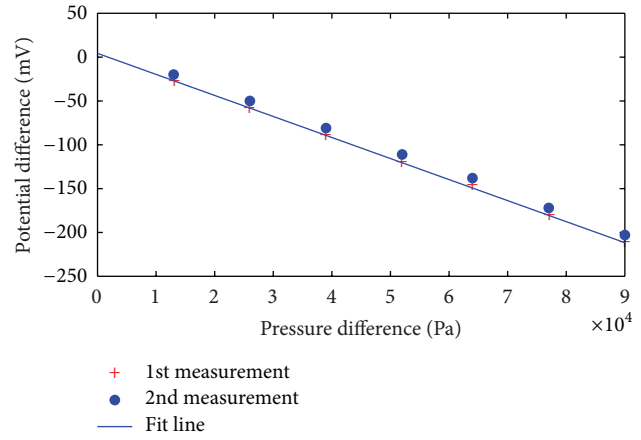

Figure 8: Measured streaming potential versus applied pressure difference for sample TS10 at two different times for equilibrium electrical conductivity of liquid of $11 \cdot 10^{-3}$ S/m.

4.2. Streaming Potential. The typical fluctuation of electrical potentials at a given pressure difference is shown in Figure 7. The final value of electric potential for each pressure difference was taken as the average value of all datapoints.

The streaming potential as a function of pressure difference was measured twice for each sample. Figure 8 shows two typical sets of measurements for sample TS10 in which the second measurement was carried out 10 h after the first one. The graph shows that there was a very small variation of streaming potentials with time (the drift is about 1 mV/h), and the straight lines fitting the data points do not go through the origin. This may be due to the electrode polarizations. However, this variation has no influence on the coupling coefficient because the slopes of straight lines are almost the same for two separate measurements.

Streaming potential coupling coefficients at 3 different electrical conductivities for sample TS10 are shown in Figure 9. From Figures 8 and 9, we see that the magnitude of the streaming potential is proportional to the driving pressure difference and is inversely proportional to the liquid electrical conductivity, as expected from (1) and (2).

From the coupling coefficients, the formation factors, and the electrical conductivities of the samples, the zeta potential of the samples can be obtained by using (2) as shown in Table 2. Because the measured coupling coefficient was always negative, the zeta potential obtained from the measurement was also negative.

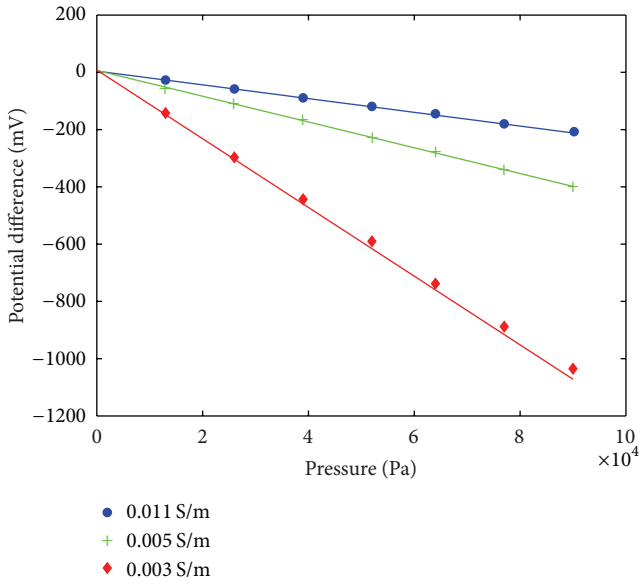

Figure 9: Example of typical runs for sample TS10 at three different liquid conductivities. We observe linear relationships between measured streaming potentials and applied pressure differences. At each electrical conductivity, the streaming potential coupling coefficient is equal to the slope of the linear trend.

4.3. Electroosmosis. Figure 10 shows the measured maximum height difference versus applied voltage for sample TS10. We observe that there is a linear relationship between the maximum height difference and the applied voltage as expected from (9) except for the last datapoint (when the applied voltage was 7.5 V). That last datapoint which deviated from the linear trend could be due to the electrolysis happening on both electrodes as mentioned in Section 3.4. Using the slope of the graph and the zeta potential obtained from streaming potential measurement, we can estimate the average pore size of the samples from (9) (see Table 2).

Because of the limitation of applied voltage, the electroosmosis measurements were only performed for sample TS10 and TS20. The height difference as a function of time carried out for sample TS10 at possible maximum applied voltage of 6 V is shown in Figure 11. The graph has an exponential curve as expected from (8). By using the exponential part of the graph, the response time in (6) was obtained (see Figure 12). From the calculated response time and parameters of the samples, the number of pores on average can be determined by electro-osmosis measurements (see Table 2).

Table 2: Calculated parameters of the samples in which ζ is the zeta potential in mV, a is average pore radius in μm, N is the average number of pores per cross-sectional area of the samples, and k_o is the permeability of the samples in m^2.

Sample	TS10	TS20	TS40	TS140	TS250	TS500	S_{sand}
ζ	−32.4	−5.2	−6.3	−12.5	−7.2	−9.1	13.7
a	2.3	3.2					
N	775×10^3	482×10^3					
k_o	0.16×10^{-12}	0.31×10^{-12}					
a from [11]	1.5	2.9	5.9	20.6	36.8	73.5	

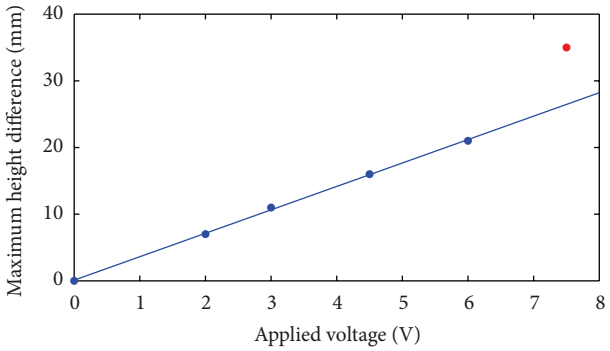

Figure 10: Maximum height difference as a function of applied voltage for sample TS10.

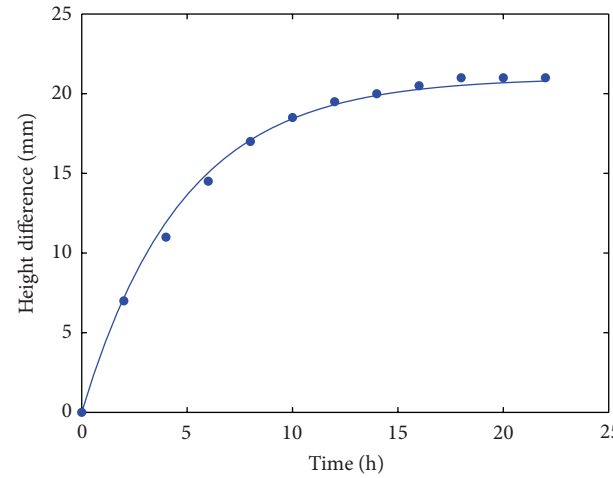

Figure 11: The dotted line is the experimental measurement of height difference as a function of time for sample TS10 at voltage of 6 V (dotted line). The solid line is fit through the datapoints.

To check the validity of the pore size estimation, we used the relationship between grain diameter and effective pore radius given by [11]

$$d = 2\theta a, \tag{12}$$

where θ is the theta transform function that depends on parameters of the porous samples such as porosity, cementation exponent, and formation factor of the samples. For the samples made of the monodisperse spherical particles arranged randomly, θ is taken to be 3.4. From pore sizes determined by the electro-osmosis measurements, permeabilities of the samples were also calculated by the model of [11] (see Table 2) as

$$k_o = \frac{a^2 \phi^{3/2}}{8}, \tag{13}$$

where ϕ is the porosity of samples. From Table 2, we see that the pore size estimated from the electro-osmosis measurement is in good agreement with that estimated from the model of [11] and that, in addition, the calculated permeabilities are in good agreement with the measured ones in Table 1.

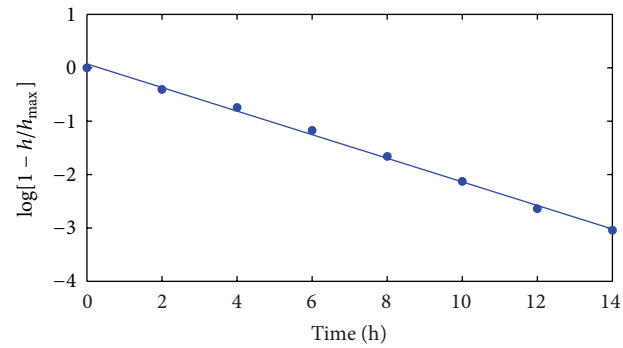

Figure 12: The slope of the straight line is equal to the reciprocal of the response time.

5. Conclusions

Streaming potential measurements have been performed for 7 unconsolidated samples fully saturated with a 10^{-3} M NaCl solution to determine the zeta potentials. Because of the limitation of the voltage one can apply, we carried out the electro-osmosis measurements for two smallest particle samples. This allows us to estimate average pore sizes of the samples as well as the number of pores these cannot be determined by a method such as the image analysis performed in [8] for very smallpore porous media. The estimated pore sizes and the measured permeabilities have been compared to those calculated from the model of [11] to check the validity of the measurements.

The comparison shows that the measured pore sizes are in good agreement with the model of [11]. If the electro-osmosis

measurements can be improved, for example, by using ion-exchange membranes or a large crosssectional area of the samples to reduce the experimental time, then this method can be applied for any kind of porous media, and it will be especially useful for very small pores.

According to [26, 27], an average value of zeta potential is about −17 mV for sands or sandstones so that the value of −13.7 mV from our measurements is within the range expected. Therefore, our approach can be effectively used to characterize porous media by using simple measurements, in particular, for very smallpore porous media that are relevant for application in the oil and gas industry.

Moreover, our streaming potential and electro-osmosis measurements also worked for the interface between a liquid and a polymeric material. The polymer may be a more promising material for electro-osmosis micropumps besides traditional materials like silica particles. The zeta potential of the polymer material that we used in this paper is a little bit smaller than that of sands or sandstones.

Acknowledgments

The authors would like to thank Professor Dr. Daniel Bonn for his very helpful suggestions and comments which have helped them to improve this paper. They also would like to thank Karel Heller for his help in improving the setups as well as measurements.

References

[1] A. Thompson, S. Hornbostel, J. Burns et al., "Field tests of electroseismic hydrocarbon detection," *SEG Technical Program Expanded Abstracts*, vol. 24, p. 565, 2005.

[2] S. S. Haines, A. Guitton, and B. Biondi, "Seismoelectric data processing for surface surveys of shallow targets," *Geophysics*, vol. 72, no. 2, pp. G1–G8, 2007.

[3] M. Strahser, L. Jouniaux, P. Sailhac, P.-D. Matthey, and M. Zillmer, "Dependence of seismoelectric amplitudes on water content," *Geophysical Journal International*, vol. 187, no. 3, pp. 1378–1392, 2011.

[4] S. Garambois and M. Dietrich, "Seismoelectric wave conversions in porous media: field measurements and transfer function analysis," *Geophysics*, vol. 66, no. 5, pp. 1417–1430, 2001.

[5] A. H. Thompson, J. R. Sumner, and S. C. Hornbostel, "Electromagnetic-to-seismic conversion: a new direct hydrocarbon indicator," *Leading Edge*, vol. 26, no. 4, pp. 428–435, 2007.

[6] S. Pride, "Governing equations for the coupled electromagnetics and acoustics of porous media," *Physical Review B*, vol. 50, no. 21, pp. 15678–15696, 1994.

[7] S. X. Li, D. B. Pengra, and P.-Z. Wong, "Onsager's reciprocal relation and the hydraulic permeability of porous media," *Physical Review E*, vol. 51, no. 6, pp. 5748–5751, 1995.

[8] T. Paillat, E. Moreau, P. O. Grimaud, and G. Touchard, "Electrokinetic phenomena in porous media applied to soil decontamination," *IEEE Transactions on Dielectrics and Electrical Insulation*, vol. 7, no. 5, pp. 693–704, 2000.

[9] S. Zeng, C.-H. Chen, J. C. Mikkelsen Jr., and J. G. Santiago, "Fabrication and characterization of electroosmotic micropumps," *Sensors and Actuators B*, vol. 79, no. 2-3, pp. 107–114, 2001.

[10] D. Bonn, S. Rodts, M. Groenink, S. Rafaï, N. Shahidzadeh-Bonn, and P. Coussot, "Some applications of magnetic resonance imaging in fluid mechanics: complex flows and complex fluids," *Annual Review of Fluid Mechanics*, vol. 40, pp. 209–233, 2008.

[11] P. W. J. Glover and E. Walker, "Grain-size to effective pore-size transformation derived from electrokinetic theory," *Geophysics*, vol. 74, no. 1, pp. E17–E29, 2009.

[12] R. J. Hunter, *Zeta Potential in Colloid Science*, Academic Press, New York, NY, USA, 1981.

[13] P. W. J. Glover and M. D. Jackson, "Borehole electrokinetics," *The Leading Edge*, vol. 29, no. 6, pp. 724–728, 2010.

[14] F. C. Schoemaker, N. Grobbe, M. D. Schakel, S. A. L. de Ridder, E. C. Slob, and D. M. J. Smeulders, "Experimental validation of the electrokinetic theory and development of seismoelectric interferometry by cross-correlation," *International Journal of Geophysics*, vol. 2012, Article ID 514242, 23 pages, 2012.

[15] L. Jouniaux, M. L. Bernard, M. Zamora, and J. P. Pozzi, "Streaming potential in volcanic rocks from Mount Pelée," *Journal of Geophysical Research B*, vol. 105, no. 4, pp. 8391–8401, 2000.

[16] A. Boleve, A. Crespy, A. Revil, F. Janod, and J. L. Mattiuzzo, "Streaming potentials of granular media: influence of the Dukhin and Reynolds numbers," *Journal of Geophysical Research*, vol. 112, no. 8, 2007.

[17] F. Reuss, "Sur un nouvel effet de l'électricité galvanique," *Mémoires de la Societé Imperiale de Naturalistes de Moscou*, vol. 2, pp. 327–336, 1809.

[18] S. Yao and J. G. Santiago, "Porous glass electroosmotic pumps: theory," *Journal of Colloid and Interface Science*, vol. 268, no. 1, pp. 133–142, 2003.

[19] C. L. Rice and R. Whitehead, "Electrokinetic flow in a narrow cylindrical capillary," *Journal of Physical Chemistry*, vol. 69, no. 11, pp. 4017–4024, 1965.

[20] R. J. S. Brown, "Connection between formation factor for electrical resistivity and fluid-solid coupling factor in Biot's equations for acoustic waves in fluid-filled porous media," *Geophysics*, vol. 45, no. 8, pp. 1269–1275, 1980.

[21] J. G. M . van der Grinten, "Tortuosity measurement and its spin-off to a new electrical conductivity standard," in *Learned and Applied Soil Mechanics*, F. B. J . Barends and P. M. P . C . Steijger, Eds., pp. 143–148, Taylor & Francis, New York, NY, USA, 2002.

[22] S. F. Alkafeef and A. F. Alajmi, "Streaming potentials and conductivities of reservoir rock cores in aqueous and non-aqueous liquids," *Colloids and Surfaces A*, vol. 289, no. 1, pp. 141–148, 2006.

[23] D. R. Lide, *CRC Handbook of Chemistry and Physics*, CRC Press, New York, NY, USA, 2004.

[24] D. H. Gray and J. K. Mitchell, "Fundamental aspects of electro-osmosis in soils," *Journal of the Soil Mechanics and Foundations Division*, vol. 93, no. 6, pp. 209–236, 1967.

[25] P. N. Sen, C. Scala, and M. H. Cohen, "A self-similar model for sedimentary rocks with application to the dielectric constant of fused glass beads," *Geophysics*, vol. 46, no. 5, pp. 781–795, 1981.

[26] L. Jouniaux, "Electrokinetic techniques for the determination of hydraulic conductivity," in *Hydraulic Conductivity—Issues, Determination and Applications*, L. Elango, Ed., InTech, 2011.

[27] L. Jouniaux and T. Ishido, "Electrokinetics in earth sciences: a tutorial," *International Journal of Geophysics*, vol. 2012, Article ID 286107, 16 pages, 2012.